Component and Cladding Wind Loads for Low-Slope Roofs on Low-Rise Buildings

Gregory A. Kopp, Ph.D., P.Eng., M.ASCE[1]; and Murray J. Morrison, Ph.D., A.M.ASCE[2]

Abstract: The component and cladding wind load provisions for low-sloped roofs on low-rise buildings in ASCE 7-10 were examined using measured pressure data from an aerodynamic database. It was found that both the design pressure coefficients and size of the roof zones in ASCE 7-10 are much smaller in magnitude than indicated by the data. The data indicate that building height is the most significant parameter affecting the size of the roof zones, while plan dimensions have a limited impact on this class of buildings. Recommendations for revised roof zones are developed, which include a modification to the shape of the corner zone, the addition of a new interior zone far from the roof edges, and a zone size definition that depends only on building height. However, even with increased roof zone sizes, the measured data indicate that the design pressure coefficients must also be increased in the corners and edges. **DOI: 10.1061/(ASCE)ST.1943-541X.0001989.**

Author keywords: Cladding and components; Wind loads; Low-rise buildings; Standards and codes.

Introduction

Wind loads on components and cladding (C&C) are larger than those acting on the main structural system. Because of the combination of turbulence in the wind and the nature of building aerodynamics, high magnitude pressures can occur over the relatively small areas associated with building components. In contrast, the main structural system responds to pressures acting on multiple surfaces such that the highly-localized, intense pressure fluctuations are attenuated by the lack of full spatial and temporal correlations. Surry et al. (2007) illustrated this point, showing the differences between point pressures and spatial averages on the roof of a low-rise building. The wind load provisions in ASCE 7-10 (ASCE 2010) capture these effects, with higher pressures being applied for the design of C&C compared to those for the main wind-force resisting system (MWFRS). In fact, the C&C provisions indicate that the pressures decrease exponentially with area such that the design pressure coefficients, GCp, for 0.93 m^2 (10 ft^2) are approximately 40% of those for 9.3 m^2 (100 ft^2), for the corner zone on low-sloped roofs of low-rise buildings (e.g., see Fig. 30.4-2A in ASCE 7-10).

The approach that has been used to obtain the design pressure coefficients for C&C in ASCE 7-10 is explained in the commentary for Chapter 30. An enveloping approach was used, whereby the worst coefficients over all wind directions were obtained, while considering that the "pressures may also vary widely as a function of the specific location on the building, height above ground level, exposure, and more importantly, local geometric discontinuities, and location of the element relative to the boundaries of the building surfaces (walls, roof lines). [These] factors were enveloped," along with the effects of wind direction [ASCE 7-10 (ASCE 2010, p. 569)].

The wind load provisions for C&C in ASCE 7-10 (ASCE 2010) for low-rise buildings with low-slope roofs are largely based on the wind tunnel studies of Stathopoulos (1979), although some other studies were also involved, as discussed in the commentary for Chapter 30 (and Chapter 28). This study, which represented a large step forward for the knowledge of wind loads on low-rise buildings, was the result of the development of the pneumatic-averaging technique whereby multiple pressure taps could be brought together to obtain spatially-averaged pressures. The results were incorporated into the ANSI A58.1-1982 (ANSI 1994) standard, which later became the 1988 version of the ASCE 7 standard [ASCE7-88 (ASCE 1990)]. Previously, in order to obtain spatial averages, temporal averaging tended to be performed over single pressure taps (e.g., Lawson 1976) to crudely estimate the effects of the spatial correlations. Today, with digital data acquisition systems and electronic transducers, more than a thousand pressure taps can be measured simultaneously, with modern studies typically using many hundreds of taps. This increase in measurement resolution is of significant importance for determining C&C loads (Surry 1999) given the exponential drop in area-averaged pressure coefficients with area.

Because of a relative lack of pressure taps Stathopoulos (1979) developed roof zones on the basis of point pressure distributions and not considerations of variations of area-averages. However, the use of this proxy data appears to be reasonable because peak (and mean) pressures decrease with distance from the roof edge, as do area averages. To determine the actual size, he "assumed that the width, z, of the edge zone is such that it includes pressures of magnitude up to 70% of the worst measured value closest to the edge" (Stathopoulos 1979, p. 158). At the time, "most codes of practice determine[d] the width . . . of the high magnitude suction loads as a function of the building width only," but he goes on to note that "the height of the building is probably another parameter which affects [the size of the edge zone]" (Stathopoulos 1979). It seems probable that the dependence on the plan dimensions arises from traditional aerodynamics, where drag and lift on airfoils depend on the chord (i.e., length). This also applies to pressures on high-rise buildings,

[1]Professor, Boundary Layer Wind Tunnel Laboratory, Faculty of Engineering, Univ. of Western Ontario, London, ON, Canada N6A 5B9 (corresponding author). E-mail: gak@blwtl.uwo.ca; gakopp@uwo.ca; gakopp.uwo@gmail.com

[2]Vice President, Insurance Institute for Business and Home Safety Research Center, Richburg, SC 29732.

Note. This manuscript was submitted on November 28, 2016; approved on September 18, 2017; published online on January 31, 2018. Discussion period open until June 30, 2018; separate discussions must be submitted for individual papers. This paper is part of the ***Journal of Structural Engineering***, © ASCE, ISSN 0733-9445.

for which many more studies existed in the late 1970s, where the local pressure coefficients on the walls are also dependent on the plan dimensions and less on the building height. Stathopoulos' data appears to have been the first use of building height for determining the roof zones. In any case, the size of the roof zone was then based on a measured length that was scaled as a proportion of the least horizontal plan dimension, W, and the height, h. This dependence of roof zones on either building height or width has remained in the standard for low-rise buildings [ASCE 7-10 (ASCE 2010)].

However, the role of building height on C&C pressures on roofs of low-rise buildings still appears to be unresolved. Lin et al. (1995) found that roof pressures were dependent on the vertical distance from the wall stagnation point to the roof edge and used building height as a proxy for this. Based on velocity field data obtained with particle image velocimetry (PIV), Akon and Kopp (2016) found that this distance (for winds normal to the wall) was at approximately $0.35h$ in a wide range of terrains, but their data also indicated that the reattachment length on the roof depended primarily on turbulence level and the wall aspect ratio, i.e., W/h (or L/h, depending on wind direction). While no plots of pressure as a function of distance from the edge are provided by Stathopoulos (1979), plots of point pressure as a function of distance from the roof edge, normalized by the building length, L, for a range of building sizes, are provided by Elsharawy et al. (2014, see their Fig. 6). Because each building has a different curve, it shows that the building length, as a minimum, does not do well minimizing the variation in the dimensional data as a function of the building geometry. In contrast, Ho et al. (2005) provide similar plots, which show that h captures the points pressure fluctuations well. Thus, the role the building geometry on the roof pressure coefficients and spatial patterns for low-rise buildings are not resolved in the literature. In fact, there has not been a systematic evaluation of the spatial variations of area-averaged pressure coefficients as a function of building geometry. The objective of this study is to examine this issue, determining the role of building geometry on the spatial patterns and magnitudes of area-averaged pressure coefficients. The large, publicly accessible, high-resolution database developed by Ho et al. (2005) is used in the current study, as described subsequently.

Experiment and Analysis Details

The experimental data obtained by Ho et al. (2005) are used in the current study. The reader is referred to that paper for details. These data, which are publically available on the internet (NIST 2008), have been extensively examined in the literature, in particular, by St. Pierre et al. (2005) who provide a detailed comparison with the data of Stathopoulos (1979). Only minimal details are provided in this paper because all significant details have already been reported.

The geometry of the buildings analyzed in this study are provided in Fig. 1. All buildings used in this paper had gable roof slopes less than or equal to 1:12 (4.8°). Two terrain conditions were examined at a scale of 1/100: open, with $z_o \sim 0.03$ m; and suburban, with $z_o \sim 0.3$ m. Considering these two terrain conditions and 19 building sizes, 38 configurations in total are used. Wall length (L) and width (W) to height (h) ratios (W/h and L/h) were varied from 1.0 to 20.6, which spans the range from the smallest possible to a very large value. Relatively few W/L ratios are included in the database, which may influence MWFRS results, but will not be relevant for the C&C loads, as discussed in the results section "Effects of Building Height and Plan Dimensions." For all tests, there were no surrounding structures. The wind directions were measured every 5 degrees over a 90-degree range. The wind direction convention is consistent with that of Ho et al. (2005), examining wind angles from 270° to 360°.

Area-averaged pressures are computed from point pressures for nonoverlapping square areas. To reduce bias due to tap resolution the current analysis required that the area under consideration had at a minimum four times the tributary area of the surrounding pressure taps. In other words, at least four pressure taps contributed to all the area-averaged pressure coefficients. Using the method described by St. Pierre et al. (2005) pressure coefficients obtained from the model scale data are converted to GCp coefficients that are directly comparable to the coefficients found in ASCE7-10 (ASCE 2010). The current study presents statistical peak coefficients rather than the absolute highest coefficient. To obtain these statistical peaks the time histories are divided into four segments. The peaks from each segment are extracted and fit with a Gumbel

Building #	W	L (ft)	h (ft)	W/h	Symbol
1/2	12.2 m (40 ft)	19.1 m (62.5 ft)	5.5 m (18 ft)	2.2	■/□
3/4	12.2 m (40 ft)	19.1 m (62.5 ft)	3.7 m (12 ft)	3.3	■/□
5/6	12.2 m (40 ft)	19.1 m (62.5 ft)	7.3 m (24 ft)	1.7	■/□
7/8	12.2 m (40 ft)	19.1 m (62.5 ft)	12.2 m (40 ft)	1.0	■/□
9/10	24.4 m (80 ft)	38.1 m (125 ft)	4.9 m (16 ft)	5.0	●/○
11/12	24.4 m (80 ft)	38.1 m (125 ft)	7.3 m (24 ft)	3.3	●/○
13/14	24.4 m (80 ft)	38.1 m (125 ft)	9.8 m (32 ft)	2.5	●/○
15/16	24.4 m (80 ft)	38.1 m (125 ft)	12.2 m (40 ft)	2.0	●/○
17/18	36.6 m (120 ft)	57.2 m (187.5 ft)	3.7 m (12 ft)	10.0	◆/◇
19/20	36.6 m (120 ft)	57.2 m (187.5 ft)	4.9 m (16 ft)	7.5	◆/◇
21/22	36.6 m (120 ft)	57.2 m (187.5 ft)	5.5 m (18 ft)	6.7	◆/◇
23/24	36.6 m (120 ft)	57.2 m (187.5 ft)	7.3 m (24 ft)	5.0	◆/◇
25/26	36.6 m (120 ft)	57.2 m (187.5 ft)	12.2 m (40 ft)	3.0	◆/◇
27/28	48.8 m (160 ft)	76.2 m (250 ft)	3.7 m (12 ft)	13.3	◀/◁
29/30	48.8 m (160 ft)	76.2 m (250 ft)	5.5 m (18 ft)	8.9	◀/◁
31/32	48.8 m (160 ft)	76.2 m (250 ft)	7.3 m (24 ft)	6.7	◀/◁
33/34	48.8 m (160 ft)	76.2 m (250 ft)	12.2 m (40 ft)	4.0	◀/◁
35/36	30.5 m (100 ft)	61.0 m (200 ft)	6.1 m (20 ft)	5.0	★/☆
37/38	30.5 m (100 ft)	61.0 m (200 ft)	9.8 m (32 ft)	3.1	★/☆

Fig. 1. Dimensions of the buildings in the current study

J. Struct. Eng., 2018, 144(4): 04018019

distribution using the Lieblein best linear unbiased estimator (BLUE) (1974) method. The peak values reported in this study are 78th percentile values from the Gumbel distribution extrapolated to 1 h using the method of Cook and Mayne (1979). In addition, the peaks presented are the enveloped values, following the procedure outlined in ASCE 7-10, as discussed earlier.

Spatial Distributions of Peak, Area-Averaged Wind Loads

Pressure Magnitudes and Critical Wind Directions

Prior to investigating the adequacy of the pressure coefficients and roof zones in the existing ASCE 7-10 provisions, the effects of building size on both the magnitude and spatial distribution of the peak, area-averaged pressure coefficients are examined. Figs. 2–5 depict the peak, area-averaged pressure coefficients, enveloped over the range of tested wind directions (270–360°) such that the lower left corner in each image is the windward corner of the building. The coefficients are worst values at each location over the range of wind directions such that the magnitudes can be compared directly to values in ASCE 7-10 (ASCE 2010); however, the spatial distribution is provided in these figures. Four different sets of plan dimensions are provided, ranging from 12.2×19.1 m to 48.8×76.2 m. Each of the figures was constructed such that the color bars for the pressure coefficients are the same and thus can be compared directly. Figs. 2–4 show areas of 0.9×0.9 m $= 0.84$ m^2 (3×3 ft $= 9$ ft^2), close to the minimum areas (0.93 m^2; 10 ft^2) considered in the ASCE 7-10 GCp curves. Fig. 5 presents results for an area of 1.2×1.2 m $= 1.5$ m^2 (4×4 ft $= 16$ ft^2) (because of tap resolution). Figures for other tributary areas indicate the same basic trends and patterns, so are not included in this paper. In addition, the zones defined by ASCE 7-10 are included as black lines. Other zone definitions are included as white lines, which will be discussed later.

Examining Figs. 2–5 it is shown that the neither the building height, h, or the plan dimensions ($W \times L$) significantly alter the values of the highest magnitude coefficients that occur over the roof surface. Similarly, the values for the smallest magnitudes are also similar, although the proportion of the roof with higher or lower magnitude loads is clearly altered by the building dimensions. Thus, the details of the spatial distribution of the peak pressure coefficients are clearly altered even though roughly the same range of values for the enveloped pressure coefficients appears in every plot. This allows examination of the spatial patterns without having to simultaneously consider different ranges of magnitudes. The effects of the building dimensions on the spatial patterns will be discussed further in the next section.

Fig. 6 shows the wind directions that resulted in the worst (i.e., enveloped) values plotted in Fig. 2, noting that a wind direction of 270° is normal to the longer wall while a wind direction of 360° is from left to right, normal to the shorter wall. Similar results arise for Figs. 3–5, but these are not shown in this paper for brevity.

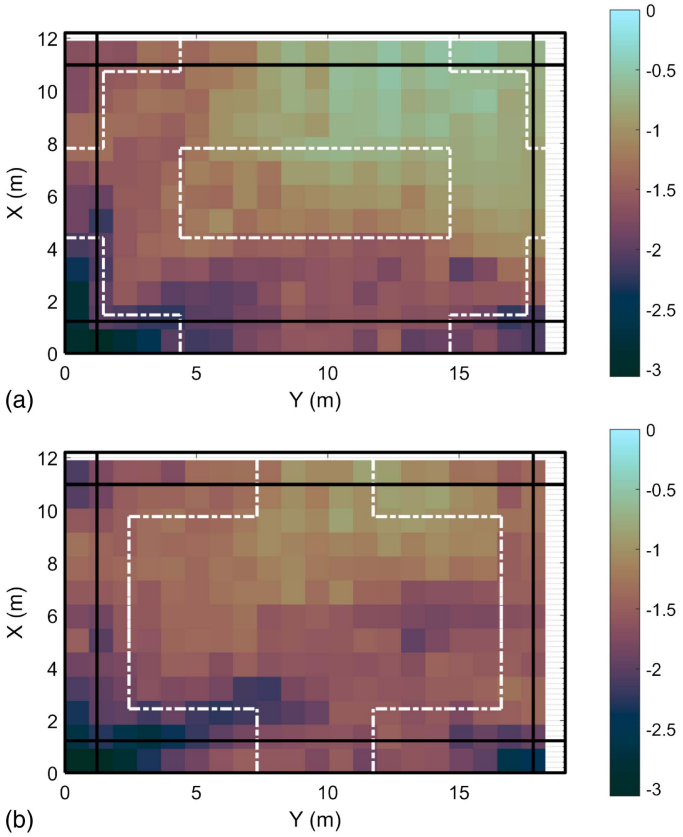

Fig. 2. Worst GCp values over a range of wind directions, 270–360° for tributary areas of 0.84 m^2 (9 ft^2) on buildings with plan dimensions of 12.2×19.1 m (40×62.5 ft) in open-country terrain: (a) $h = 7.3$ (24 ft); (b) $h = 12.2$ (40 ft); the black lines correspond to the ASCE 7-10 definition for the roof zones while the white dashed lines represent proposed roof zones

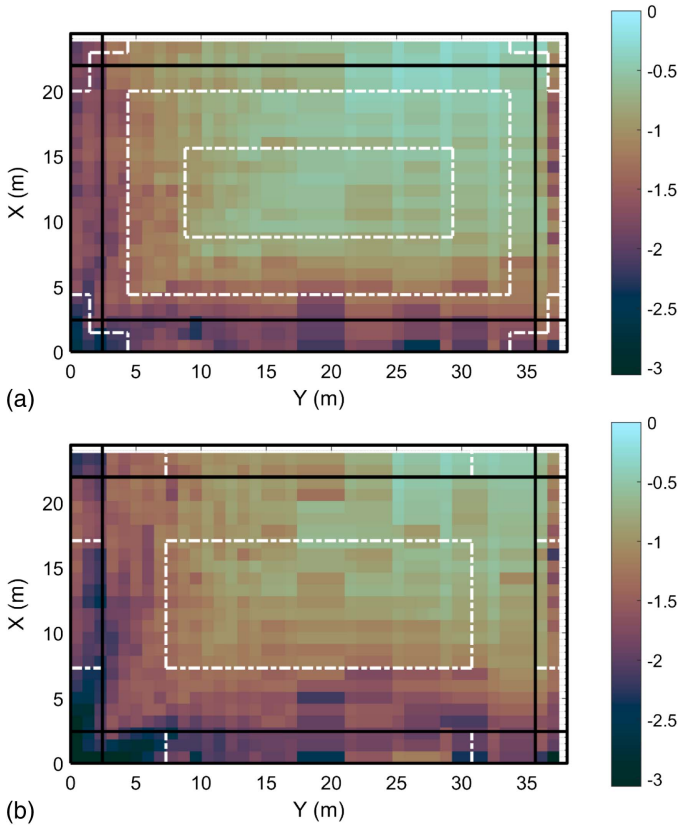

Fig. 3. Worst GCp values over a range of wind directions, 270–360° for tributary areas of 0.84 m^2 (9 ft^2) on buildings with plan dimensions of 24.4×38.1 m (80×125 ft) in open-country terrain: (a) $h = 7.3$ (24 ft); (b) $h = 12.2$ (40 ft); the black lines correspond to the ASCE 7-10 definition for the roof zones while the white dashed lines represent proposed roof zones

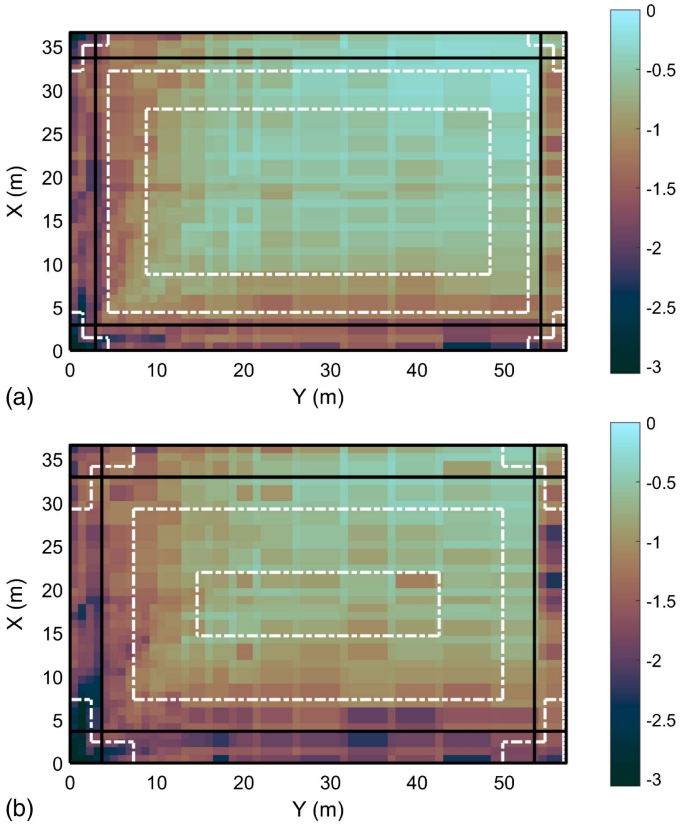

Fig. 4. Worst GCp values over a range of wind directions, 27–360° for tributary areas of 0.84 m^2 (9 ft^2) on buildings with plan dimensions of 36.6×57.2 m (120×187.5 ft) in open-country terrain: (a) $h = 7.3$ (24 ft); (b) $h = 12.2$ (40 ft); the black lines correspond to the ASCE 7-10 definition for the roof zones while the white dashed lines represent proposed roof zones

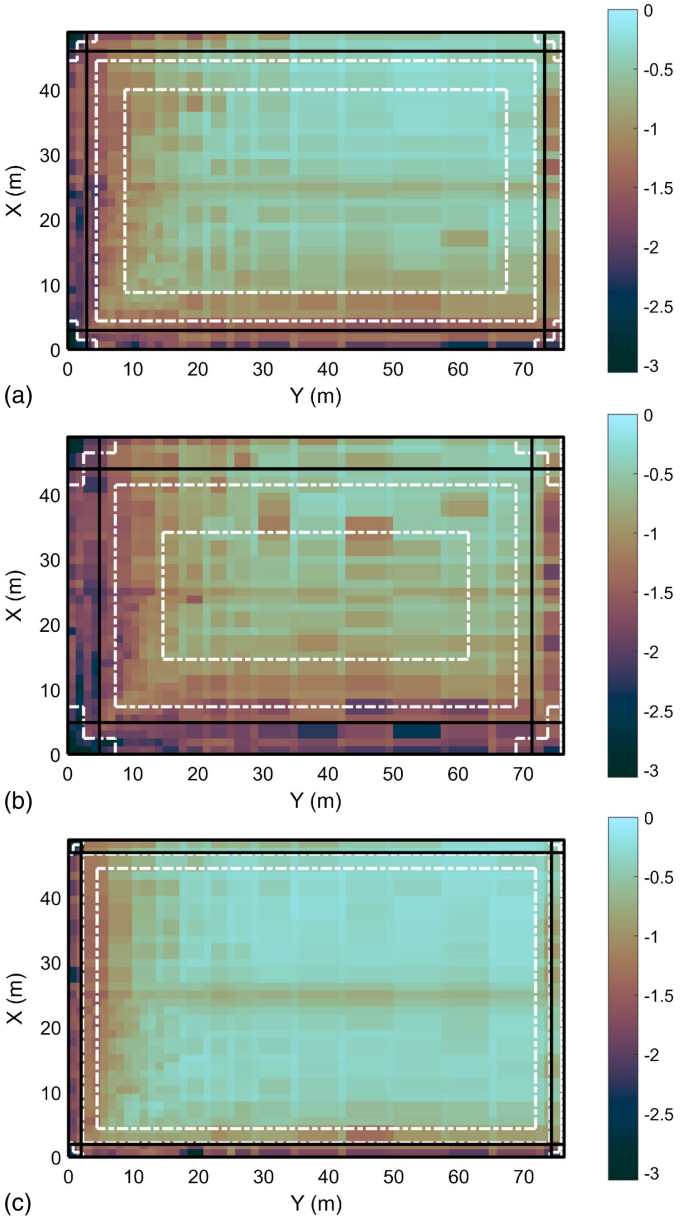

Fig. 5. Worst GCp values over a range of wind directions, 270–360° for tributary areas of 1.5 m^2 (16 ft^2) on buildings with plan dimensions of 48.8×76.2 m (160×250 ft) in open-country terrain: (a) $h = 7.3$ (24 ft); (b) $h = 12.2$ (40 ft); (c) $h = 3.7$ m (12 ft); the black lines correspond to the ASCE 7-10 definition for the roof zones while the white dashed lines represent proposed roof zones

The figure indicates that the overall pattern of critical wind directions is split in two if one draws a 45-degtee line from the windward corner into the roof, with significantly different values on either side of the line. One implication of this is that the W/L ratio is not going to be a critical parameter for the relatively small areas of importance for C&C loads. In particular, between the edge of the shorter wall and this 45-degree line, the critical wind directions are mostly between roughly 310° and 360°; between the roof edge of the longer wall and this 45-degree line, the critical wind directions are mostly between 270° and 300°. Very close to the corner and edge of the roof along the short wall, the critical directions are 310–340°, which are caused by the corner vortices (Banks and Meroney 2001) that act along a large portion of this side of the roof. Near the corner and edge along the longer wall, similar patterns are observed with critical directions near 300°, i.e., approximately 30° from wall normal. Thus, along edges near the corners, oblique wind directions tend to cause the worst coefficients and the area-averaged pressure coefficients tend to be a function of the distance from the corner, as shown in Fig. 2.

In the interior of the roof, away from the windward corner, the critical wind directions generally shift to more wall normal directions, i.e., 340–360° or 270–290°, although Fig. 2(a) indicates that cornering winds control far from the corner near the leeward corner of the roof for the lower building height. Outside of the windward corner region where the cornering/oblique winds control, the values of the pressure coefficients tend to be smaller and become a function mostly of distance from the edge. This is most clear in the figures with relatively large plan dimensions and small roof heights, such as Figs. 3(a), 4(a), and 5(a), but will be examined subsequently in greater detail. These latter figures also indicate that the enveloped pressure coefficient becomes relatively uniform and unchanging further from the roof edges, typically at approximately 10 m from the edges for buildings with $h = 7.3$ m [and approximately 15 m for $h = 12.2$ m in Figs. 3(b), 4(b), and 5(b)].

Effects of Building Height and Plan Dimensions

Because the magnitudes of the area-averaged pressure coefficients are broadly similar for all buildings examined, the details of the spatial patterns that depend on the building size need to be examined in order to define zone boundaries for design. Specifically,

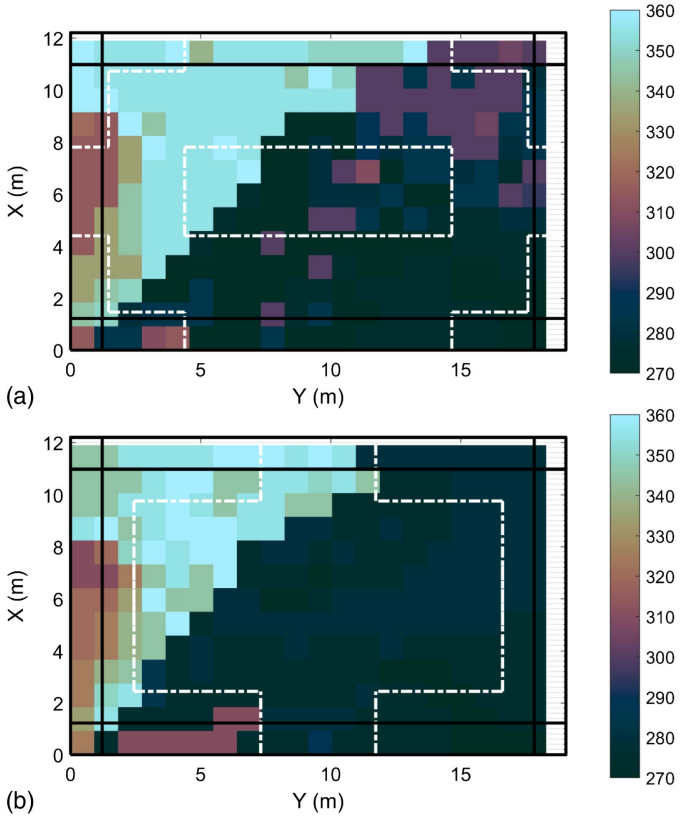

Fig. 6. Critical wind directions, for tributary areas of 0.84 m^2 (9 ft^2) on buildings with plan dimensions of 12.2×19.1 m (40×62.5 ft) in open-country terrain: (a) $h = 7.3$ (24 ft); (b) $h = 12.2$ (40 ft); the black lines correspond to the ASCE 7-10 definition for the roof zones while the white dashed lines represent proposed roof zones

the effects of building height and plan dimensions on the spatial distributions of roof pressures will be investigated. Because the magnitudes of the pressures are similar over all buildings, it is helpful to examine fixed pressure levels and compare the positions for these, for the range of buildings. The current discussion will focus on two levels, $GCp = -2.5$, which represents large magnitude pressures near the windward corner, and -0.5, which represents lower magnitude pressures near the interior.

To examine the effects of height, each of Figs. 2–5 is for a fixed plan size. Consider Fig. 2. For $GCp = -2.5$, Fig. 2(a) indicates that, for $h = 7.3$ m, the pressures at this level extend in either direction from the windward corner for approximately 5 m along the edge in an L or V shape. For $h = 12.2$ m, these values have a similar shape but extend from the windward corner approximately 8 m along the longer wall, but only for 3–4 m along the shorter wall. For $GCp = -0.5$, this magnitude begins at distances of approximately 7 to 8 m from the corner in either direction for $h = 7.3$ m. For $h = 12.2$ m, this value is not common, with a small region near $(x, y) \sim (10\text{ m}, 10\text{ m})$, as shown in Fig. 2(b). Based on this, one can conclude that the spatial patterns for the two buildings of common plan dimension are not similar and roof height must be a significant parameter in the spatial distribution of the enveloped pressure coefficients. Examining Figs. 3–5 reveals a similar conclusion.

To examine the effects of plan dimensions, Figs. 2(a), 3(a), 4(a), and 5(a) are for fixed roof heights of $h = 7.3$ m (24 ft), with least horizontal dimensions of $W = 12.2$, 24.4, 36.6, and 48.8 m (40, 80, 120, and 160 ft), yielding W/h ratios of 1.7, 3.3, 5.0, and 6.7, respectively. Figs. 2(b), 3(b), 4(b), and 5(b) are for roof heights of $h = 12.2$ m (40 ft) such that the W/h ratios are 1.0, 2.0, 3.0, and 4.0, respectively. As noted previously, for $GCp = -2.5$, Fig. 2(a) indicates that, for $h = 7.3$ m, this magnitude of pressures extends in either direction from the windward corner for approximately 5 m along the edge in an L or V shape. In Fig. 3(a), which has plan dimensions that are twice as large as those for Fig. 2(a) but the same roof height, these pressures also extend for approximately 5 m along each edge. Similarly, for Figs. 4(a) and 5(a), the $GCp = -2.5$ values extend out in the range of 4–7 m. As shown in Fig. 2(a), $GCp = -0.5$ values begin at distances of approximately 7 to 8 m from the corner in either direction. Examining Figs. 3(a), 4(a), and 5(a), these pressures occur at approximately the same position on the roof. Similar observations can be made for Figs. 2(b)–5(b), but with different locations for these pressures. It is also evident that, when examining the spatial pressure distributions as a whole, they are similar when building height is held constant and other plan dimensions are examined. In addition, it is observed that similar magnitude pressures cover larger dimensional areas of the roof when the building height is larger.

The overall spatial patterns of the area-averaged pressure coefficients and critical wind directions (1) are similar for low-rise buildings with low-sloped roofs of the same building height; (2) with the highest magnitude pressures in the windward corner, where pressures tend to decrease with distance from the corner and are dependent on oblique wind directions; (3) with high magnitude pressures on the edge, which decrease in proportion to the distance from the edge and are dependent on wind directions normal the wall; and (4) the areas of the roof with high magnitude pressures are larger for higher buildings than for lower ones. Plan dimensions play a secondary role to the spatial distributions of the enveloped, area-average pressure coefficients.

The effects of the plan dimensions and building height on the spatial patterns are of importance because these are parameters that are used to determine zone sizes in building codes. For low-rise buildings, ASCE 7-10 determines the size of the roof zones by considering both the plan dimensions (i.e., the least horizontal dimension) and the roof height, while for buildings above 18.3 m (60 ft) (Fig. 30.6-1) they depend only on the plan dimensions. From Fig. 30.4-2A of ASCE 7-10, the dimension of the edge zone, a, is defined as "10% of least horizontal dimension or $0.4h$, whichever is smaller, but not less than either of 4% of least horizontal dimension or 0.9 m (3 ft)." So, for low-rise buildings that are large enough that the 0.9 m (3 ft) criterion does not apply [which occurs when $W \geq 9$ m (30 ft) and $h \geq 2.3$ m (7.5 ft)], there are three possible constraints that control a, which depend on the aspect ratio of the shorter wall, W/h. Fig. 7 graphically depicts how the edge zone size, a, is determined as a function of W/h. In this figure, a is plotted nondimensionally as a/h. The three constraints are all plotted, viz, $a/h = 0.1W/h$, $a/h = 0.4$ and $a/h = 0.04W/h$, along with the ASCE definition. As shown, the least horizontal dimension, W, sets the size of the edge zone for buildings with $W/h \leq 4$, via the constraint $a = 0.1W$, and for $W/h \geq 10$, via the constraint $a = 0.04W$. The roof height sets the value of a for wall aspect ratios between these two bounds, i.e., in the range $4 \leq W/h \leq 10$. For large aspect ratios, as $W/h \to \infty$, the size of the edge zone is increased without bound because $a = 0.04W$. This does not appear to be reasonable based on both dimensional and physical grounds and it is unclear as to why the building length would be the controlling parameter for very large plan dimensions. At the other bound, $W/h \to 0$, note that $W/h \leq 1$ is no longer a low-rise building shape because such buildings are taller than wide. One might expect transitions in behavior in the region of $W/h \sim 1$.

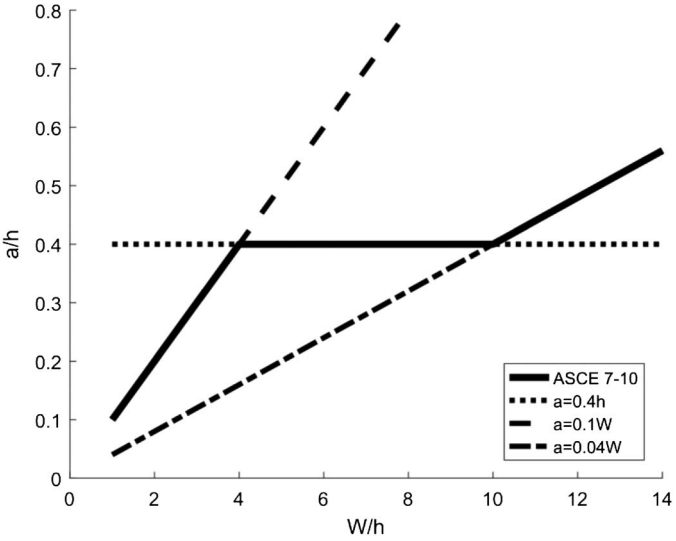

Fig. 7. Graphical depiction of the corner/edge zone size, a, in ASCE 7-10

The data in Figs. 2–5 span a range of the aspect ratio W/h from 1 to 13.3, providing an opportunity to assess how the spatial patterns of the area-averaged pressure coefficients vary with building dimensions. For Figs. 2(b)–5(b), ASCE 7-10 suggests that the edge zone should be largest for $W/h = 4$ [Fig. 5(d)] and smallest for $W/h = 1$ [Fig. 2(b)]. In fact, the ASCE 7-10 provisions suggest that the edge zone for $W/h = 4$ should be four times larger than for $W/h = 1$. As observed earlier, the roof edge zone does not have a strong dependence on the plan dimensions; rather, the building height is clearly controlling the size of the edge zones in the measured data. Thus, the functional dependence for a, as given in Fig. 30.4-2A in ASCE 7-10, does not capture the variations of the roof loads in terms of the role of the least horizontal dimensions. In order to determine the actual size of the edge, the magnitudes of the pressure coefficients also need to be examined, as considered in the following sections.

Effects of Terrain Conditions

In the experimental database used in the current analysis, both open country ($z_o = 0.03$ m) and suburban ($z_o = 0.3$ m) terrains were considered. Because the C&C coefficients apply in both, and most buildings are located in suburban terrain, the effects of terrain need to be considered. Fig. 8 depicts the spatial distributions of the enveloped coefficients for the same buildings as in Fig. 3, but for suburban terrain. Both the magnitude of the coefficients, and the spatial distribution can be compared and careful examination indicates that both the magnitude and distribution of the coefficients are similar, noting slight variations in the coefficients because of the turbulence levels and the stochastic nature of peak pressures. In fact, the degree of similarity between the two figures is remarkable, indicating that the peak pressures and the square of the gust speed are changing in the same way such that the coefficients remain essentially unchanged. All building shapes examined had this similarity such that terrain is not a significant parameter for the coefficients over the range tested.

Magnitude of the Enveloped *GCp* Values and Variation with Distance from Roof Edge

As discussed previously, the enveloped pressure coefficients, GCp, tend to decrease with distance from the edge over the bulk of the roof, except for the windward corner, where they decrease with respect to distance from the corner. In order to determine appropriate zone sizes, it is important to understand how the enveloped pressure coefficients vary with distance from the roof edge for a range of tributary areas. Figs. 9–11 depict the enveloped GCp values as a function of distance from the nearest edge, Δ, for tributary areas of 1.5, 7.5, and 18.2 m^2 (16, 81, and 196 ft^2), respectively. These figures represent a synthesis of the data presented in Figs. 2–5 and Fig. 8, but also include the data from all buildings in Fig. 1 in both terrains. Note that for Fig. 9, fewer buildings are included due to tap

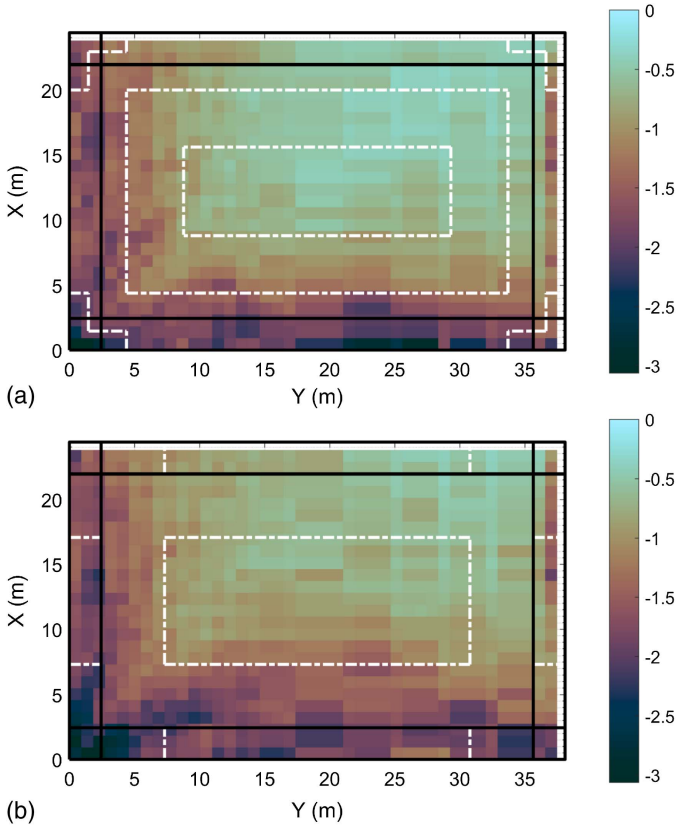

Fig. 8. Worst GCp values over a range of wind directions, 0–90° for tributary areas of 0.84 m^2 (9 ft^2) on buildings with plan dimensions of 24.4 × 38.1 m (80 × 125 ft) in suburban terrain: (a) $h = 7.3$ m (24 ft); (b) $h = 12.2$ m (40 ft); the black lines correspond to the ASCE 7-10 definition for the roof zones while the white dashed lines represent proposed roof zones

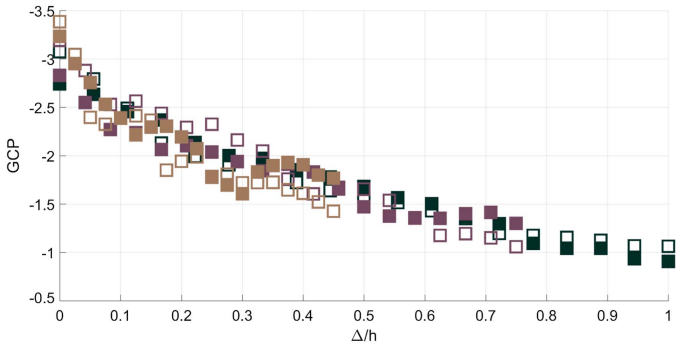

Fig. 9. Enveloped GCp values as a function of nondimensional distance from the roof edge, Δ/h, for tributary areas of 1.5 m^2 (16 ft^2)

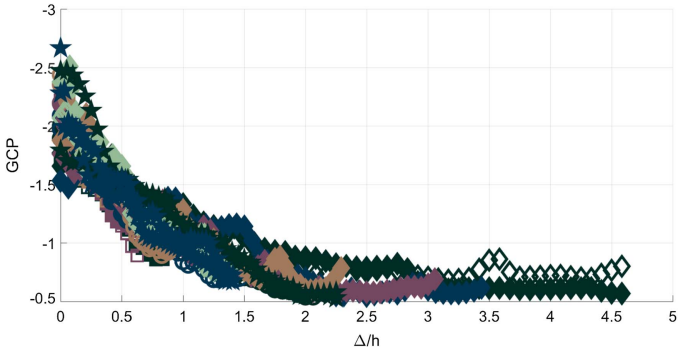

Fig. 10. Enveloped GCp values as a function of nondimensional distance from the roof edge, Δ/h, for tributary areas of 7.5 m^2 (81 ft^2)

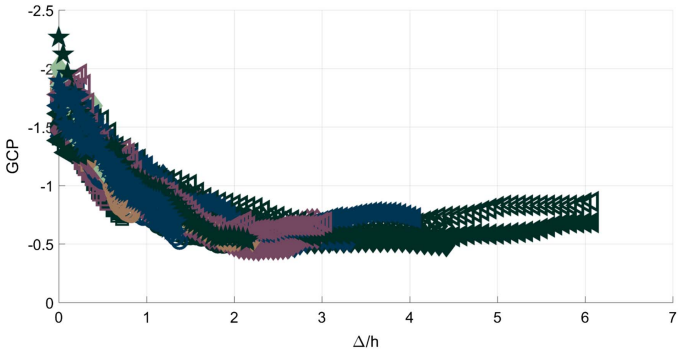

Fig. 11. Enveloped GCp values as a function of nondimensional distance from the roof edge, Δ/h, for tributary areas of 18.2 m^2 (196 ft^2)

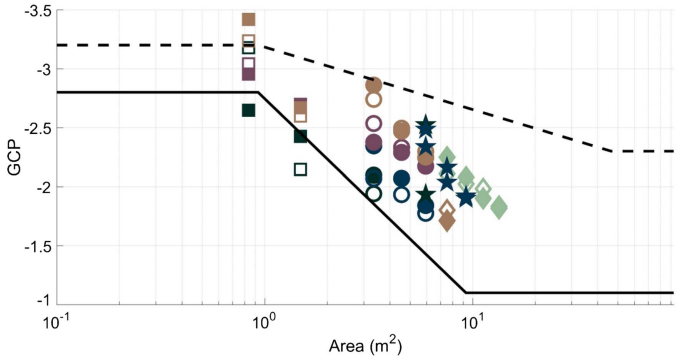

Fig. 12. Comparison of the data from the NIST database with the provisions in ASCE 7-10 for roof Zone 3 (corner); the solid line represents GCp for $h < 18.3$ m (60 ft) while the dashed line represents GCp from the all-heights provisions

resolution and this study's requirement on the number of pressure taps contributing to the area average. Based on the discussion in the previous section, the distance from the edge is normalized by the building height, h. All three figures show similar trends with decreasing magnitudes of coefficients for larger distances from the edge. The majority of the change is within $\Delta/h < \sim 1$. The use of h provides a reasonable parameter to collapse the curves onto a single line, although there is significant scatter. Note that the scatter in the normalized curves propagates further from the edge for larger tributary areas in Figs. 10 and 11, perhaps because there are more data, but it may also be because the current investigation used nonoverlapping areas and the area averages have larger spatial extents, e.g., the area of 18.2 m^2 (196 ft^2), i.e., a side length of 4.3 m (14 ft), extending edge effects further into the roof compared to, for example, the 1.2 m (4 ft) side length of the 1.5 m^2 (16 ft^2) areas. The degree of collapse of the data onto a single curve is significant, given that the range of W/h is from 1.0 to 13.3. In other words, the effects of the plan dimensions clearly have a lesser impact on the area-averaged roof pressures for these low-sloped roofs on low-rise buildings than the building height. The plan dimensions do play a subtle role, which may have larger effects near the corner and edge as $\Delta/h \to 0$, as shown in Figs. 2–5. Such plan dimension effects may be caused by the intensity of the corner vortices being dependent on wall size [see discussion in SEAOC-PV2 (SEAOC 2012)] and reattachment lengths of the separated flow being dependent on the wall aspect ratios, W/h or L/h (Akon and Kopp 2016). However, for $\Delta/h > \sim 0.5$, the statistical variations in the peak coefficients mask the effects of plan dimension, and building height is the most important geometric parameter. Finally, while there is some scatter of the data between open country and suburban terrains for each building, no clear trend is apparent in Figs. 9–11.

Figs. 9–11 also indicate that the pressure coefficients decrease monotonically with Δ/h, with the values reaching an asymptotic limit between $\Delta/h = 1.5$ and 2.0. Thus, the interior (field) of the roofs experience the lowest values. The continuous variation of pressures implies that the choice of zone sizes is arbitrary, except in the far interior (i.e., $\Delta/h > \sim 1.5$). Based on these curves, one could structure design provisions without zones, using functions that depend on roof height and tributary area. Such provisions would be a series of curves, like those in these figures, one for each tributary area. However, maintaining the current structure of the provisions in ASCE 7 implies making a choice between the pressure levels in the zones, and the size of the zones. This is discussed in detail in the following section.

Assessment of Existing ASCE 7-10 Provisions

In this section, the aerodynamic data are systematically compared to the provisions of ASCE 7-10 (ASCE 2010). The provisions for low-rise buildings with nearly flat roofs in Fig. 30.4-2A define three roof zones, which are labeled as 1 (interior), 2 (edge), or 3 (corner). The edge/corner zone size is defined using the parameter, a, which was discussed previously. In each zone, enveloped pressure coefficients, GCp, that depend on tributary area are provided, with highest coefficients in the corner zone and lowest in the interior. These are presented in Figs. 12–14. Also included in these figures are the provisions for buildings with $h > 18.3$ m (60 ft), referred to as all-heights in the current paper from Fig. 30.6-1 of ASCE 7-10. The roof zones in the all-heights provisions are different from the low-rise, with an L-shaped corner zone, and a defined as "10% of least horizontal dimension, but not less than 3 ft (0.9 m)." Figs. 12–14 show that the design pressure coefficients are larger for buildings of all-heights (Fig. 30.6-1) than they are for the low-rise buildings (Fig. 30.4-2A). The measured, enveloped data for each building are also presented for comparison with these provisions.

For roof Zone 3 (corner), Fig. 12 shows that the measured data mostly fit between the two sets of requirements. For a tributary area of 0.84 m^2 (9 ft^2) near the ASCE 7 cut-off of 0.93 m^2 (10 ft^2), almost all of the measured data are larger in magnitude than $GCp = -2.8$. For larger areas, the magnitudes drop, fitting between the two sets of provisions. Thus, the low-rise provisions (Fig. 30.4-2A) are smaller (in magnitude) than the measured data,

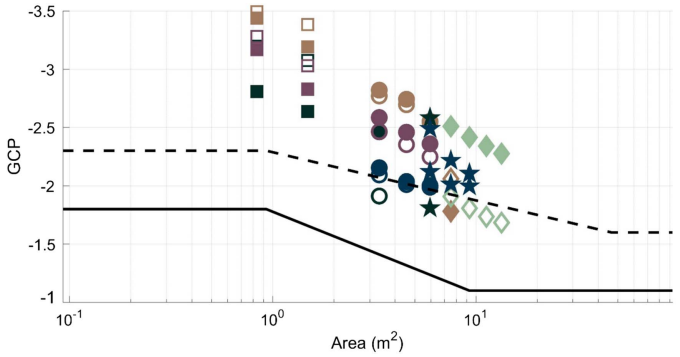

Fig. 13. Comparison of the data from the NIST database with the provisions in ASCE 7-10 for roof Zone 2 (edge); the solid line represents GCp for $h < 18.3$ m (60 ft) while the dashed line represents GCp from the all-heights provisions

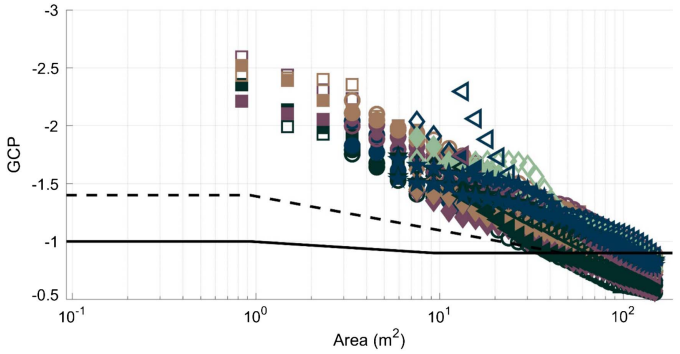

Fig. 14. Comparison of the data from the NIST database with the provisions in ASCE 7-10 for roof Zone 1 (interior); the solid line represents GCp for $h < 18.3$ m (60 ft) while the dashed line represents GCp from the all-heights provisions

while the all-heights provisions (Fig. 30.6-1) tend to be higher than the data.

Figs. 13 and 14 indicate that measured coefficients are substantially above both sets of provisions for roof Zone 2 (edge) and 1 (interior), respectively. For roof Zone 2 (edge), Fig. 13 shows that, for most tributary areas, the measured wind loads in the edge zone are not only higher than both sets of provisions, they also tend to be higher than those in roof Zone 3 (corner). The reason for this can be found in Fig. 2(b), which shows that the highest magnitude measured loads extend from the corner zone into the edge and interior zones, indicating that the size and shape of the existing zones are not adequately capturing the aerodynamic data. In fact, Fig. 14 shows that for Zone 1 (interior) the range of GCp values is only slightly smaller than those for Zone 3 (corner) because high magnitude values extend significantly further into the roof than the current provisions suggest for all buildings examined. For the buildings in Fig. 2, the size of the corner/edge zones, a, is controlled by the least-horizontal-dimension clause in both the low-rise and all-heights provisions, and is 1.2 m (4 ft) for these buildings, which is clearly too small.

One question to be raised with regard to ASCE 7-10 is whether the roof zones can be improved by the elimination of the plan dimension clause in the definition of the edge/corner zone size, a, i.e., use $a = 0.4h$. Examining Figs. 9–11 it is clear that the results would be improved by making the zone sizes dependent on the building height (the actual GCp versus area plots are not shown in this paper for brevity); however, the magnitude of the measured pressure coefficients are also larger than those in the low-rise provisions of Fig. 30.4-2A. Simply changing the roof zones is not sufficient to yield an accurate match between the data and the current low-rise provisions.

Proposed Modifications to ASCE 7

Modified Roof Zones

Wind load provisions for components and cladding depend on both the area-averaged pressure coefficients and the spatial patterns and distribution of the pressure coefficients. In ASCE 7-10, there are three roof zones with differences in pressure coefficients for tributary areas of 0.93 m^2 (10 ft^2) in the low-rise provisions between edge and corner zones of 35% and interior to edge zones of 44%, as shown in Figs. 12–14. For the all-heights method, the differences at 0.93 m^2 (10 ft^2) are 28 and 39%, respectively. Similar changes in magnitude were used for the roof zones for roof-mounted solar arrays, as discussed by Kopp (2014).

As shown in Figs. 9–11, the peak area-averaged pressure coefficients vary monotonically with distance from the edge of the roof. Because of this continuous variation, the choice of zone sizes is arbitrary and dependent on the differences in loads between zones that one wishes to have. The only exception to this would be for a zone in the field of the roof beyond the asymptotic limit where the pressures only have limited variations. In the current study, the choice was made to try to maintain the existing pressure coefficients and pressure differentials between zones to the extent possible, while keeping track of the zone sizes so that the corner and edges can be as small as possible. The all-heights pressure coefficients in Fig. 30.6-1 were used as a guide because it was shown earlier that these would be a better starting point.

To obtain the GCp curves for each zone first requires the actual zone sizes to be set. The zoning patterns have been derived from the loading patterns observed in Figs. 2–5, 8, and 9–11, particularly with respect to the observation that the pressure patterns are primarily dependent on building height, h. Fig. 15 depicts the resulting roof zones, which have an L-shaped corner with a width of $0.2h$ from the edge of the roof and lengths of 0.6 h along the roof edge. The edge zone was defined to be $0.6h$ wide, from the roof edge. This is larger than the current edge zone size in ASCE 7-10 because zones with $a = 0.4h$ could not be made to work with respect to the interior zone pressure coefficients. In addition, the data support a fourth zone to capture the low magnitude coefficients far from the roof edge (Figs. 9–11). Because the roof zones depend on only h, different plan dimensions, W and L, or more precisely, different W/h and L/h ratios lead to buildings with 2, 3, or 4 roof zones. Fig. 15(a) provides a fully nondimensional plot of roof zones, while the four possibilities are depicted in Figs. 15(b–e). For low buildings with $W/h > 2.4$, all four roof zones will be present. However, for $1.2 < W/h < 2.4$ the building plan dimensions are not large enough, relative to the height, for the new (field of the roof) zone to appear. For buildings that are approaching cube-like dimensions, with $W/h < 1.2$ and $L/h < 1.2$, there are only two zones because the width of the building is such that the corner zones meet on all four walls.

To compare the impact of these proposed zones, Figs. 2–5 and 8 indicate the current roof zones for low-rise buildings based on the requirements of Fig. 30.4-2A (black lines) and the proposed zones from Fig. 15 (dashed white lines). Fig. 2(b) provides an example that has two roof zones while Fig. 5(c) provides an example with

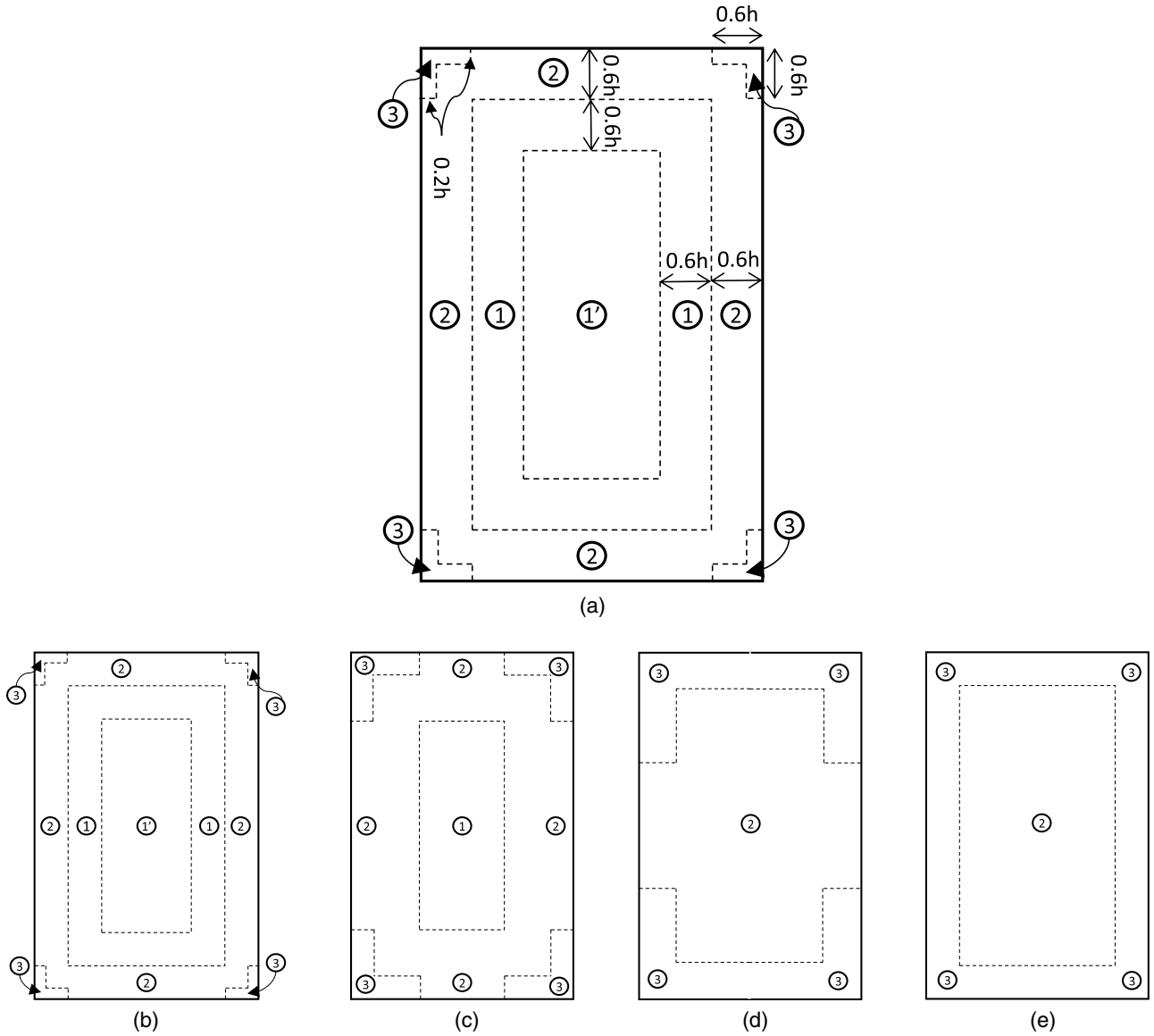

Fig. 15. (a) Proposed roof zones sketched nondimensionally for buildings with (b) $W/h > 2.4$; (c) $1.2 < W/h < 2.4$; (d) $W/h < 1.2$, $L/h > 1.2$; (e) $L/H < 1.2$, $W/h < 1.2$

four roof zones. For all buildings examined in the current study, the proposed sizes for Zones 3 (corner) and 2 (edge) are larger than for ASCE 7-10. In fact, only for buildings with $W/h > 15$ would the existing standard lead to larger corner/edge zone sizes. To have smaller zones would require larger design pressure coefficients in all zones, as implied by the data in Figs. 12–14. However, for buildings with large plan dimensions relative to the height (e.g., Figs. 4 and 5) the loads in areas away from the edge of the roof are lower than those in ASCE 7-10, as observed by comparing Figs. 9–11 with Figs. 12–14. These data support the creation the new zone for the field of the roof (labeled as Zone 1′), and represent a large proportion of the roof surface when W/h is large. Fig. 5(c) provides an example of this from the current data set.

For all buildings examined, contours of the enveloped GCp suggest that an L-shaped Zone 3 (corner) is best for capturing the highest magnitude pressures. This corner zone shape is similar to that specified for buildings with heights greater than 18.3 m (60 ft) in Fig. 30.6-1. Based on the current data, if a square-shaped area is used, a corner zone with dimensions of $0.6 \times 0.6h$ would be highly conservative over a large portion (over 50%) of this zone. Alternatively, a square corner zone with smaller dimensions would require substantially larger GCp values in Zone 2 (edge) leading to significant conservatism over significant portions of the roof.

Enveloped Pressure Coefficients

Figs. 16–19 depict the enveloped data using the proposed zones in Fig. 15, as well as the ASCE 7-10 pressure coefficients from Figs. 30.4-2A and 30.6-1. A comparison of Fig. 12 with Fig. 16 shows that this change has a significant effect on the corner zone loads because the higher loads from the previous edge zone are now in the corner. As a result, the enveloping values are larger for Zone 3 (corner) with the proposed zone definition. As before, the low-rise GCp curve of Fig. 30.4-2A has design wind loads substantially below those indicated by the experimental data, while the curve in Fig. 30.6-1 for all-heights is a more reasonable match for all data but is conservative for tributary areas larger than approximately 5 m^2 (~50 ft^2).

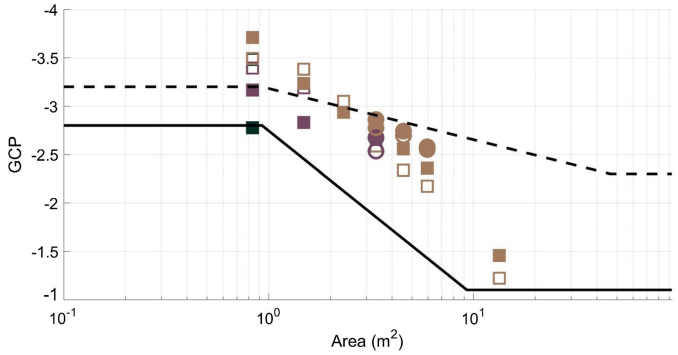

Fig. 16. GCp values for roof Zone 3 (corner) using the proposed roof zones; the solid line represents GCp for $h < 18.3$ m (60 ft) while the dashed line represents GCp from the all-heights provisions

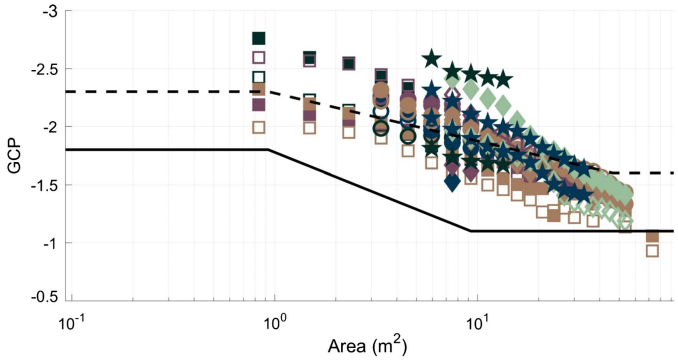

Fig. 17. GCp values for roof Zone 2 (edge) using the proposed roof zones; the solid line represents GCp for $h < 18.3$ m (60 ft) while the dashed line represents GCp from the all-heights provisions

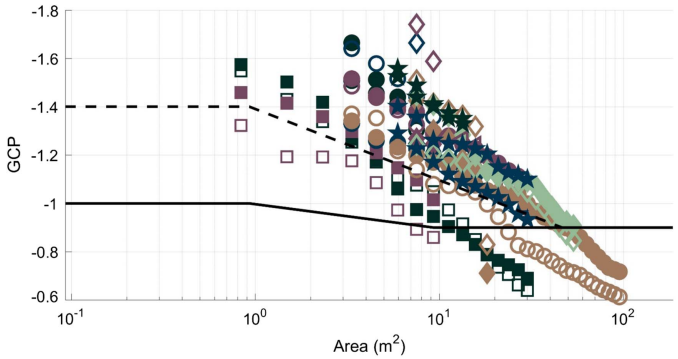

Fig. 18. GCp values for roof Zone 1 (interior) using the proposed roof zones; the solid line represents GCp for $h < 18.3$ m (60 ft) while the dashed line represents GCp from the all-heights provisions

Fig. 17 indicates that, for the new Zone 2 (edge), the experimental observations are now scattered on either side of the provisions for all-heights, but continue to be well above the low-rise provisions. Importantly, the pressure coefficients in Zone 2 are less than those in Zone 3, which indicates that the new zone definitions have been effective at eliminating the problem of larger observed pressures in Zone 2. If the all-heights pressure coefficients were to be used for design, it would imply that the loads are underestimated for many buildings. Referring once again to Figs. 2–5 clarifies the

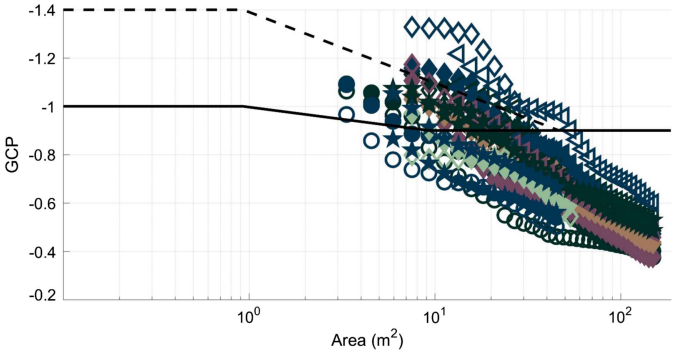

Fig. 19. GCp values for roof Zone 1′ (interior–field of roof) using the proposed roof zones; the solid line represents GCp for $h < 18.3$ m (60 ft) while the dashed line represents GCp from the all-heights provisions

choices involved. For example, in Fig. 5(c) it is shown that pressure coefficients near the boundary of Zone 1′ (field of roof) are different along the short and long walls, with higher values near the boundary near the short wall compared to for the long wall. Other figures show similar effects. Figs. 2–5 and 9–11 also indicate how the choice of zone directly affects the choice of design pressure coefficients because of the generally monotonic decrease as a function of distance from the roof edge with the trade-off being a balance between the size of the zone and the resulting magnitude of the coefficients. There is a choice to be made about where to draw the curves and zone boundaries for use in design, depending on the probability of nonexceedance that one desires. Similar questions arise from the data for Zones 1 and 1′ in Figs. 18 and 19, respectively. The measured data indicate that both the roof zone sizes and pressure coefficients must be increased in ASCE 7-10 (ASCE 2010).

Conclusions

The wind load provisions for low-sloped roofs on low-rise buildings in ASCE 7-10 were examined using the NIST Aerodynamic Database. The primary findings are

- The spatial patterns of the area-averaged pressure coefficients, enveloped over wind direction, are primarily dependent on roof height. Thus, when the spatial dimensions of the roof are normalized by the building height, the resulting patterns are similar. This indicates that the roof zone sizes and shapes for low-rise buildings should be a function of building height;
- The enveloped, area-averaged pressure coefficients on the roof decrease monotonically with distance from the roof edge. These measured coefficients are substantially larger in magnitude than those in Fig. 30.4-2A of ASCE 7-10 (ASCE 2010), with larger values spanning larger areas of the roof;
- In addition, the roof zones sizes and shapes in ASCE 7-10 are too small such that the measured pressure coefficients are higher in the edge zone than the corner zone, contrary to the values suggested by the provisions. This is due to high magnitude pressures extending further into the roof than suggested by the current provisions; and
- Recommendations for new zone sizes and shapes were developed that attempted to minimize both the changes in zone size and the magnitude of the design pressure coefficients. The most significant changes are that the corner zone is changed to an L shape, a new field-of-the-roof zone is established to capture

low pressure coefficients far from the roof edge, and that the size of the zones is dependent only on the building height and not the plan dimensions.

Acknowledgments

The authors are grateful to the many colleagues on the ASCE 7-16 Wind Loads Subcommittee (WLSC) who provided feedback, comments, and support for this work, particularly, Drs. Tim Reinhold and Peter Vickery who helped with the ballot item on the WLSC, along with Dr. Jon Peterka who provided a detailed, independent review.

References

Akon, F. A., and Kopp, G. A. (2016). "Mean pressure distributions and reattachment lengths for roof-separation bubbles on low-rise buildings." *J. Wind Eng. Ind. Aerodyn.*, 155, 115–125.

ANSI (American National Standards Institute). (1994). "Minimum design loads for buildings and other structures." *ANSI A58.1-1982*, New York.

ASCE. (1990). "Minimum design loads for buildings and other structures." *ASCE 7-88*, Reston, VA.

ASCE. (2010). "Minimum design loads for buildings and other structures." *ASCE 7-10*, Reston, VA.

Banks, D., and Meroney, R. N. (2001). "A model of roof-top surface pressures produced by conical vortices: Model development." *Wind Struct.*, 4(3), 227–246.

Cook, N. J., and Mayne, J. R. (1979). "A novel working approach to the assessment of wind loads for equivalent static design." *J. Wind Eng. Ind. Aerodyn.*, 4(2), 149–164.

Elsharawy, K., Galal, K., and Stathopoulos, T. (2014). "Comparison of wind tunnel measurements with NBCC 2010 wind-induced torsion provisions for low- and medium-rise buildings." *Can. J. Civ. Eng.*, 41(5), 409–420.

Ho, T. C. E., Surry, D., Morrish, D., and Kopp, G. A. (2005). "The UWO contribution to the NIST aerodynamic database for wind loads on low buildings. 1: Basic aerodynamic data and archiving." *J. Wind Eng. Ind. Aerodyn.*, 93(1), 1–30.

Kopp, G. A. (2014). "Wind loads on low-profile, tilted, solar arrays placed on large, flat, low-rise building roofs." *J. Struct. Eng.*, 10.1061/(ASCE)ST.1943-541X.0000825, 04013057.

Lawson, T. V. (1976). "The design of cladding." *Build. Environ.*, 11(1), 37–38.

Lieblein, J. (1974). "Efficient methods of extreme-value methodology." *NBSIR 74-602*, National Bureau of Standards, Washington, DC.

Lin, J. X., Surry, D., and Tieleman, H. W. (1995). "The distribution of pressure near roof corners of flat roof low buildings." *J. Wind Eng. Ind. Aerodyn.*, 56(2–3), 235–265.

NIST. (2008). "NIST aerodynamic database." ⟨http://fris2.nist.gov/winddata/⟩ (Oct. 07, 2016).

SEAOC (Structural Engineers Association of California). (2012). "Wind design for low-profile solar photovoltaic arrays on flat roofs." *SEAOC-PV2*, Sacramento, CA.

Stathopoulos, T. (1979). "Turbulent wind action on low-rise buildings." Ph.D. thesis, Univ. of Western Ontario, London, ON, Canada.

St. Pierre, L. S., Kopp, G. A., Surry, D., and Ho, T. C. E. (2005). "The UWO contribution to the NIST aerodynamic database for wind loads on low buildings. 2: Comparison of data with wind load provisions." *J. Wind Eng. Ind. Aerodyn.*, 93(1), 31–59.

Surry, D. (1999). "Wind loads on low-rise buildings: Past, present and future." *Proc., 10th Int. Conf. Wind Engineering*, International Association for Wind Engineering, Copenhagen, Denmark, 105–114.

Surry, D., Sinno, R. R., Nail, B., Ho, T. C. E., Farquhar, S., and Kopp, G. A. (2007). "Structurally effective static wind loads for roof panels." *J. Struct. Eng.*, 10.1061/(ASCE)0733-9445(2007)133:6(871), 871–885.